JACS
JOURNAL OF THE AMERICAN CHEMICAL SOCIETY

Communication

[Ag(SR)]$^-$: The 'Golden' Silver Nanoparticle

Chakra P Joshi, Megalamane S. Bootharaju, Mohammad J. Alhilaly, and Osman M. Bakr

J. Am. Chem. Soc., **Just Accepted Manuscript** • DOI: 10.1021/jacs.5b07088 • Publication Date (Web): 31 Aug 2015

ACS Publications

Journal of the American Chemical Society is published by the American Chemical Society. 1155 Sixteenth Street N.W., Washington, DC 20036

$[Ag_{25}(SR)_{18}]^-$: The 'Golden' Silver Nanoparticle

Chakra P. Joshi,[†] Megalamane S. Bootharaju,[†] Mohammad J. Alhilaly,[†] and Osman M. Bakr*,[†]

[†]Division of Physical Sciences and Engineering, Solar and Photovoltaics Engineering Research Center, King Abdullah University of Science and Technology (KAUST), Thuwal 23955-6900, Saudi Arabia

Supporting Information Placeholder

ABSTRACT: Silver nanoparticles with an atomically precise molecular formula $[Ag_{25}(SR)_{18}]^-$ (–SR: thiolate) are synthesized and their single-crystal structure is determined. This synthesized nanocluster is the only silver nanoparticle that has a virtually identical analogue in gold, *i.e.*, $[Au_{25}(SR)_{18}]^-$, in terms of number of metal atoms, ligand count, super-atom electronic configuration, and atomic arrangement. Furthermore, both $[Ag_{25}(SR)_{18}]^-$ and its gold analogue share a number of features in their optical absorption spectra. This unprecedented molecular analogue in silver to mimic gold offers the first model nanoparticle platform to investigate the centuries-old problem of understanding the fundamental differences between silver and gold in terms of nobility, catalytic activity, and optical property.

Silver and gold have contrasting physical and chemical properties despite their similarity in atomic size, structure, and bulk-lattice. Throughout the ages, humankind was captivated by the properties of these lustrous metals. However, only in the last century or so have scientists been able to investigate the underlying fundamental differences between silver and gold and their origin down to the nanoscale. This pursuit was made possible through advancements in nanofabrication techniques, which enabled the synthesis of metal nanostructures and their confinement in organic shells.[1,2] These advancements accentuated the differences in chemical properties between gold and silver. For example, gold nanoparticles were found to be effective catalysts for several reactions such as carbon monoxide oxidation[3] and aldehydes reduction,[4] and their noble behavior makes them relatively biocompatible[5,6] and thus useful for biomedicine[6,7]. On the other hand, silver nanoparticles were found to exhibit much lower catalytic utility and are quite cytotoxic; hence, they are used often in antibacterial surface coatings.[1,8]

The discovery of nanoclusters, which are atomically precise nanoparticles, have brought forth a nanoparticle system, whose properties are well defined, modeled, and explained.[1,2,9-13] In the past ten years, the nanocluster community has made great strides in the synthesis, isolation, and crystal structure determination of a remarkable number of gold species,[2,9,10] but only a few species of silver[1,11,12,14,15]. Prominent examples of gold are Au_{25},[5,9,10] Au_{38},[5,16] Au_{102},[17] and Au_{133}[18,19] while a handful of silver clusters crystallized are Ag_{44},[11,12] Ag_{32},[20] Ag_{29},[15] Ag_{21},[14] Ag_{16},[20] and Ag_{14}[21]. Unfortunately, no pure silver cluster published so far has a matching analogue in gold, making a direct comparison between gold and silver challenging and inconclusive. Attempts towards materializing such analogues by increasing dopant amount[12,22-24] were limited by the accessible sites within clusters, for which exchange could occur without destroying the original underlying structure. For instance, while doping Au_{25} with Ag Kumara et al.[22] found 12 exchangeable positions in Au_{25} without compromising the cluster's structural integrity. Further increase in dopant concentration led to cluster decomposition. This difficulty may stem from the stability of silver clusters; gold clusters have various sizes with the same ligand[2] whereas silver clusters have a much more constrained relationship between a size and a ligand type[25].

Herein we present the synthesis, design, and crystal structure of the silver nanocluster $[Ag_{25}(SR)_{18}]^-$ – an analogue of $Au_{25}(SR)_{18}$. This is the first silver nanoparticle with an exact analogue in gold in terms of size, composition, superatom electronic configuration, charge, and the crystal structure. The discovery of this model system provides a platform for the direct and unambiguous comparison of the properties of silver and gold nanoparticles, thus enabling theoretical developments for investigating fundamental differences in their catalytic and physicochemical properties.

Typically, the synthesis (see the Supporting Information (SI)) of $[Ag_{25}(SR)_{18}]^-$ involves the use of 2,4-dimethylbenzenethiol ($HSPhMe_2$), a ligand with two bulky methyl groups that were found critical for tuning the product cluster size to Ag_{25}. Replacement of these two bulky methyl groups with fluorine resulted in a product with Ag_{44}[12] absorption features (Figure S1). Synthesis of Ag_{25} involves a methanolic solution of $AgNO_3$ that was mixed with the ligand $HSPhMe_2$ in dichloromethane to form a yellow insoluble silver thiolate mixture. This mixture was then reduced using aqueous $NaBH_4$ in the presence of tetraphenylphosphonium bromide ($PPh_4^+Br^-$). The counterions (PPh_4^+) are necessary for a successful synthesis of Ag_{25} clusters because they are negatively charged, and it is a lack of such counterions during synthesis that produced large plasmonic nanoparticles. Finally, synthesized Ag_{25} clusters were purified, dried, and made readily available into non-polar and polar-aprotic solvents such as dichloromethane (DCM), dimethylformamide (DMF), dimethylsulfoxide (DMSO), and toluene for further study.

The final purified product was analyzed by UV-vis spectroscopy to reveal an absorption onset at ~850 nm and a highly structured optical spectrum unique to Ag_{25} (Figure 1). The Ag_{25} was also found to exhibit luminescence in the near-infrared region ~850 nm. Typically, silver clusters are brown to red[11,26-28] and usually are associated with that color, but the color resemblance between Ag_{25} cluster and that of large plasmonic Ag nanoparticles may have delayed its discovery. To naked eyes, the purified Ag_{25} cluster solution appeared yellow (Figure 1, inset) similar to Au_{25} prepared (Figure S2) using the same thiol. The similarity in absorption features of the purified Ag_{25} with those of Au_{25} synthesized using various thiols (Figures S1 and S2) is quite interesting. The optical features of the purified Ag_{25} bear a

resemblance to both Ag and Au cluster features. For example, Ag_{25} shares the same intense ~490 nm peak of Ag_{44}[11,12] and Ag_{35}[26] (Figure S3). It is possible that the appearance of a common ~490 nm peak in these Ag clusters is coincidental. On the other hand, Ag_{25} has also a broad peak ~675 nm similar to Au_{25} and other peaks below 450 nm region making Ag_{25} acquire character of Au. The clues to such optical behavior may be found in the Ag_{25} crystal structure (*vide infra*).

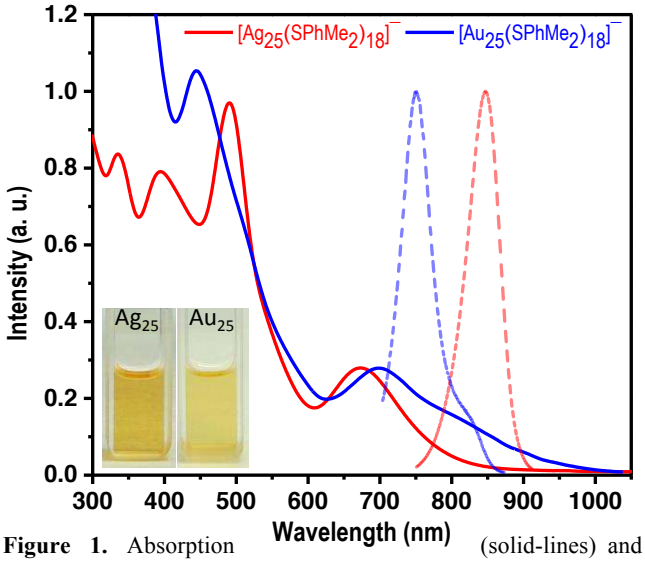

Figure 1. Absorption (solid-lines) and normalized emission (dotted-lines) spectra of $[Ag_{25}(SPhMe_2)_{18}]^-$ and $[Au_{25}(SPhMe_2)_{18}]^-$ in DCM. Inset: photographs showing actual color of the synthesized Ag_{25} and Au_{25} with the same ligand $HSPhMe_2$.

We then characterized the purified product with matrix-assisted laser desorption ionization (MALDI) mass spectrometry (MS) using trans-2-[3-(4-tertbutylphenyl)-2-methyl-2-propenylidene] malononitrile (DCTB) as the matrix. Of the several fragment peaks evident from the MALDI spectrum (Figure S4), all peaks appear to have originated from the same source molecule with a mass-to-charge-ratio m/z ~ 5167. Electrospray ionization (ESI) MS of the same purified product also identified a single intense peak at m/z ~ 5167 attributed to negatively charged $Ag_{25}(SPhMe_2)_{18}$ (Figure 2). The single peak in the ESI MS indicates the purity and the atomic monodispersity of the synthesized product. Experimental data matched well with the simulation (see inset) for the molecular formula $[Ag_{25}(SPhMe_2)_{18}]^-$, indicating that the entire cluster possesses a unit negative charge. Further analysis of our purified product in the positive ionization mode found the PPh_4^+ cation (Figure S4), confirming that the cluster core is indeed negatively charged; thus, establishing the purified product's identity as $[Ag_{25}(SPhMe_2)_{18}]^-PPh_4^+$.

In order to investigate the crystal structure of the synthesized cluster with single-crystal X-ray diffraction, we crystallized the clusters from a DCM/hexane mixture at 4 °C over 2-7 days. Dark black crystals (Figure S5) were grown from solutions that were suitable for single-crystal measurements (see the SI for details).

The crystal structure of the purified product resolved the PPh_4^+ counterion and a few solvent molecules associated with Ag_{25} (Figure 3a-c). This observation provides an unambiguous determination of the identity of the purified clusters as $[Ag_{25}(SPhMe_2)_{18}]^-$ with PPh_4^+ as the sole counterion, further confirming our predictions deduced from the mass spectrometry. The cluster's metallic core comprises one Ag at the center surrounded by another 12Ag atom forming a compact icosahedral

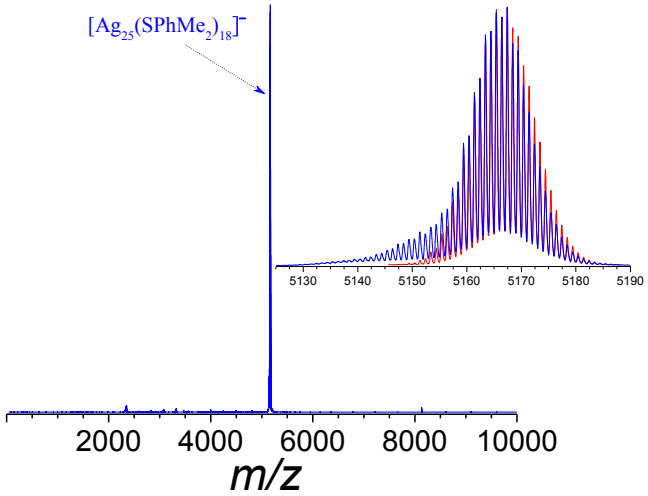

Figure 2. Negative mode ESI MS of $[Ag_{25}(SPhMe_2)_{18}]^-$ clusters in DCM, inset: overlap of the experimental data (blue) and the simulated spectrum (red) for $[Ag_{25}(SPhMe_2)_{18}]^-$.

core of Ag_{13} with approximate I_h symmetry (Figure 3d-f). The remaining 12 non-icosahedral Ag atoms of Ag_{25} can be viewed as occupying 12 triangular faces of the icosahedron core (note: an icosahedral core comprises 20 triangular faces, 30 edges, and 12 vertices). A careful look at the locations of these 12 non-icosahedral Ag atoms in the crystal structure (Figure 3e, grey) could reveal that nine of these atoms occupy the nine triangular face centers of the Ag_{13} core whereas the remaining three can be found facing away from triangular face centers. This type of atomic arrangement (or distortion) at the metallic core may be unique to Ag_{25} and is perhaps the only notable difference from Au_{25} clusters, where all 12 non-icosahedral Au atoms seem to lie at the center of triangular faces of the icosahedral core.[10]

The non-hollow metallic core of Ag_{25} (Figure 3f) has not been observed with other pure mono-thiolated Ag clusters, such as Ag_{44},[11,12] which has a hollow icosahedral core of Ag_{12}. Although there are reports of non-hollow icosahedral Ag cores, these Ag clusters are either protected with a dithiophosphate[14] or a mixed thiol-phosphine[15,20,21] ligand system. It is not yet clear how this hollow/non-hollow core associated with Ag clusters manifest itself in the overall cluster properties.

As mentioned earlier, there are 12 non-icosahedral Ag atoms surrounding the Ag_{13} core of $[Ag_{25}(SPhMe_2)_{18}]^-$. They are connected with 18S (from 18 thiol ligands) that can be divided into six Ag_2S_3 groups. Each Ag_2S_3 group contains two anchoring and one non-anchoring S to the Ag_{13} core (Figure 3d). Both the anchoring S and the non-anchoring S with two-non-icosahedral Ag of a group creates a V-shaped –S–Ag–S–Ag–S– motif. Six such motifs around the Ag_{13} core may define a pseudo-octahedral or a quasi-T_h symmetry present in Ag_{25} that satisfies the bonding requirements of the Ag present on the surface of the icosahedral core. This symmetry and bonding could explain why Au_{25} and Ag_{25} have similar optical transitions[29] and properties.

It is surprising to find that Ag_2S_3 motifs exhibit a one-dimensional structure. This is the first example of protective units in a Ag cluster orienting this way rather than being decorated with either three-dimensional Ag_2S_5 protective units[11,12] or two-dimensional Ag–S sheets as in silver-thiolate complexes[30]. Potentially, the shape of protective groups could be tuned to elicit desired properties in clusters. In addition, the observation of one-dimensional motifs in Ag_{25} may counter the view that the Ag_2S_5 motifs of Ag_{44}[11,12] are ubiquitous in silver, unlike in gold clusters where Au_2S_3 motifs appear to be the dominant configurations.[10,2]

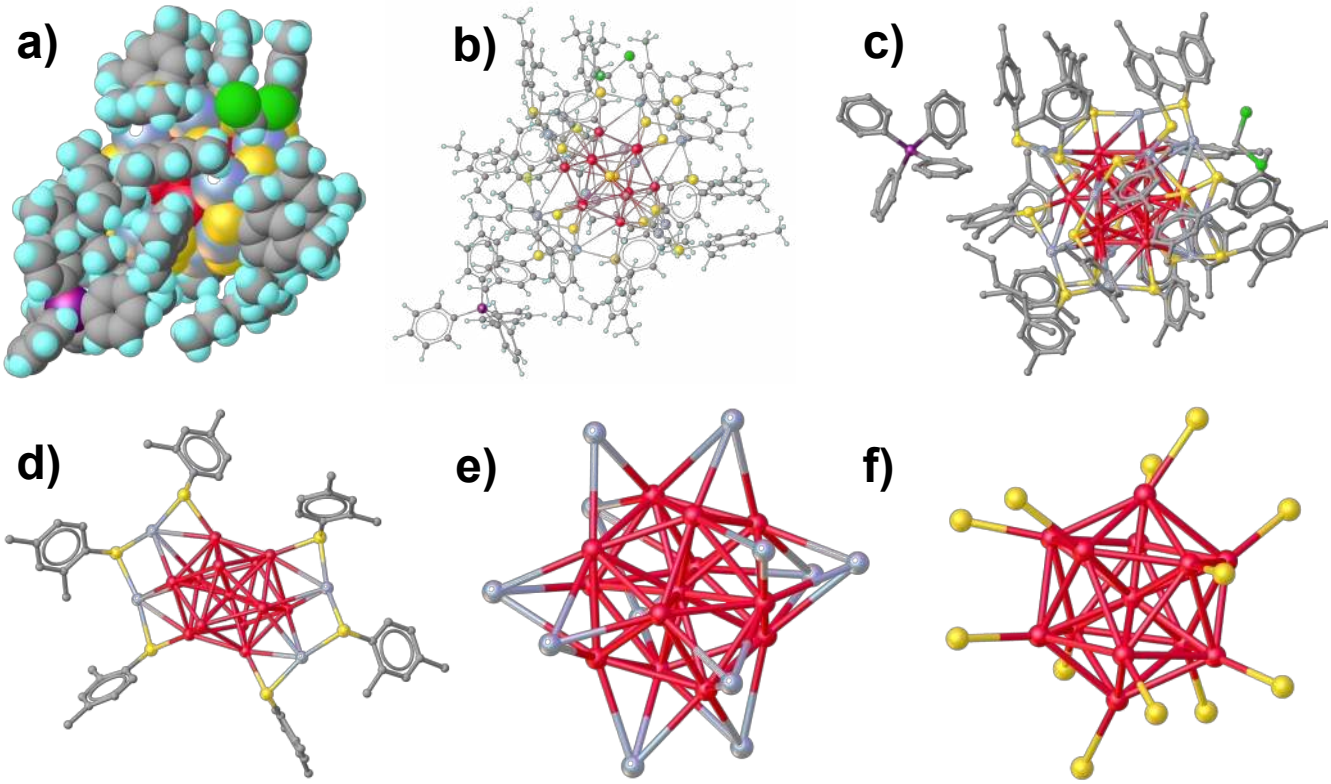

Figure 3. X-ray structure of the $[Ag_{25}(SPhMe_2)_{18}]^-$ crystal. **(a)** A space-filling view of the cluster with cations and solvent molecules (color scheme below). Ball-and-stick views of **(b)** the entire cluster showing $SPhMe_2$ ligand, PPh_4^+ counterion, and solvent molecules; **(c)** entire cluster without hydrogen atoms; **(d)** a pair of Ag_2S_3 motifs surrounding the icosahedral Ag_{13} core and the orientation of ligands in the motif; **(e)** the position of 12 non-icosahedral Ag with respect to the icosahedral core; and **(f)** the non-hollow 13-atom Ag icosahedral core and the bonding of vertices in the icosahedral with S from ligand molecules. Color scheme: red, icosahedral core Ag; light grey, non-icosahedral Ag; yellow, sulfur; dark grey, carbon; green, chlorine; pink, phosphorus, and cyan blue, hydrogen atoms.

The crystal structure of the cluster reveals inter-motif interactions in $[Ag_{25}(SPhMe_2)_{18}]^-$ due to the proximity of Ag with anchoring S. Only three motifs could be observed to participate in such interactions. Recall that three Ag atoms are oriented away from triangular face centers. It is these Ag atoms that seem to facilitate inter-motif interactions. The inter-motif Ag–S bond distance was found to be 2.803–2.947 Å, larger than any other Ag–S distance (2.382–2.445 Å) observed within a motif. This type of weak inter-motif interaction is not observed in Au_{25}, which might explain why most gold clusters have one-dimensional protective motifs[2,10]. In addition, inter-motif interactions in Ag_{25} might give a clue to how three-dimensional motifs in larger Ag clusters, such as Ag_{44},[11,12] come into being from such interactions present in smaller clusters.

Further analysis of the crystal structure reveals inter-motif interactions via the phenyl rings of the ligands, where all the six motifs of Ag_{25} are engaged. These phenyl ring interactions (~face-to-face, 3.49–3.68 Å) occur via π–π stacking and seem to influence ligands orientation, minimizing repulsions between bulky methyl groups. The 12 ligands of Ag_{25} are observed to participate in such interactions — six ligands from two motifs, four from another two, and two from remaining two motifs (Figure S6). It is plausible that the distortions in Ag_{25} motifs may have been created to accommodate these ligand-ligand π–π interactions that have a profound effect on the Ag_{25} crystal structure and stability.

Stability is an important aspect for all metal clusters. The crystal structure of Ag_{25} reveals the presence of solvent molecules (e.g., DCM and hexane). These solvent molecules may coordinate with the cluster to enhance its long-term stability. The existence of four larger pockets or voids in Ag_{25} cluster (Figure 3a-c) may provide coordination sites for solvents. We observed the stability of Ag_{25} in toluene, DMF, and DMSO solvents and found that DMSO provided the best longevity of the cluster (Figure S7), likely it is a good coordinating solvent. Extreme drying of these clusters can cause the loss of coordinating solvents, which could enable them to aggregate into large plasmonic Ag nanoparticles.

To make a direct comparison on the stability of Ag_{25} and Au_{25} we synthesized them using the same ligand $HSPhMe_2$ (see the SI). We found that the $[Ag_{25}(SPhMe_2)_{18}]^-$ was relatively less stable than its analogue $[Au_{25}(SPhMe_2)_{18}]^-$ under ambient conditions. However, at 4 °C (inside fridge), Ag_{25} clusters were stable for weeks similar to Au_{25}, indicating that the stability of Ag_{25} is temperature-dependent. We predict that with further investigation and the right choice of ligand, the stability of Ag_{25} could be improved to match or even exceed that of Au_{25}. For instance, in previous work, we demonstrated the year-long ambient stability of Ag_{44} clusters with the $HSPhNO_2COOH$ ligand[31], a stability that could not be obtained with other protecting ligands[11,32,12,25].

Soon after the discovery of Au_{25} clusters, Aikens presented theoretical insight into a hypothetical Ag_{25} cluster[25,29] using time-dependent density functional theory (TDDFT). Aikens showed that the icosahedral core may be viewed as a Ag_{13}^{+5} core surrounded by six $Ag_2S_3^-$ motifs leading to an eight electron formal charge on the entire Ag_{25} cluster. This type of electronic distribution can also be understood by calculating the number of free electrons (n_e) present in $[Ag_{25}(SR)_{18}]^-$ *via* the relationship $n_e = Nv\text{-}M\text{-}z$,[33,34] where N is the number of Ag atoms, v is the valence (1 for Ag), M is the number of mono-thiol ligands, and z is the overall cluster charge. Thus, the number of free electrons in $[Ag_{25}(SPhMe_2)_{18}]^-$, can be found by $n_e = 25\times1\text{-}18\text{-}(-1) = 8$,

corresponding to the stable superatom electronic configuration $1S^2|1P^6|$, where S and P represent the angular momentum quantum numbers of the superatomic orbitals, and vertical lines represent shell-closure with a large gap between highest occupied molecular orbitals (HOMO) and lowest unoccupied molecular orbitals (LUMO).[33] The predicted stability of $[Ag_{25}(SPhMe_2)_{18}]^-$ is also in accordance with the stability curve for the ligand-protected metal clusters.[34]

Some similarities in the optical features of Ag_{25} between its theoretical and experimental absorption spectra, such as a broad peak at ~675 nm compared to ~756 nm, for experimental and theoretical results[25,29], respectively, may originate from HOMO-LUMO transitions, where HOMO is believed to be triply degenerate and LUMO doubly degenerate. Similarly, the experimental ~490 nm peak (theory, ~498 nm) could also be due to HOMO-1 to LUMO transitions. Possibly, the shift observed between experimental and theoretical data[29] may be caused by a lack of the actual atomic coordinates for simulating the Ag_{25} spectrum. Furthermore, the simulated spectrum does not take into account the inter-motif interactions and distortions in the actual crystal structure of $[Ag_{25}(SPhMe_2)_{18}]^-$, factors that may cause some shift and the appearance/disappearance of peaks in the simulated spectrum. Ligand effects[35,36] may also explain the differences between experimental and simulated spectra, an angle we intend to investigate in our future work. The implication from the theoretical study[25,29] that Au and Ag have comparable optical and electronic behaviors is supported by our experimental observations here, indicating silver may be able to acquire the properties of gold and vice versa. The future of silver or gold nanomaterials with such duality is perhaps not too far-fetched despite underlying differences between Ag and Au due to relativistic effects, stemming from the high atomic number of the latter. The integration of dual-characteristics in nanomaterials has the potential to contribute considerable advancements toward the future of nanoscience and technology.

In summary, we synthesized and completely characterized $[Ag_{25}(SPhMe_2)_{18}]^-$, the first silver cluster with an exact analogue in gold, i.e., $[Au_{25}(SPhMe_2)_{18}]^-$. This work serves as a model platform for developing a theoretical and experimental framework for the direct conclusive comparison of properties of gold and silver. The possibility of manufacturing such analogues in other metal/non-metal systems would open channels for their technological use and for understanding the evolution of materials from atomic to bulk scale.

ASSOCIATED CONTENT

Supporting Information

Synthetic methods of Ag_{25} and Au_{25}, characterization, stability study, single-crystal X-ray analysis, and other relevant experimental information. This material is available free of charge via the Internet at http://pubs.acs.org.

AUTHOR INFORMATION

Corresponding Author

*osman.bakr@kaust.edu.sa

Notes

The authors declare no competing financial interests.

ACKNOWLEDGMENT

The authors acknowledge using KAUST resources and core-lab facilities.

REFERENCES

(1) Zheng, K.; Yuan, X.; Goswami, N.; Zhang, Q.; Xie, J. *RSC Adv.* **2014**, *4*, 60581.
(2) Jin, R. *Nanoscale* **2015**, *7*, 1549.
(3) Li, G.; Jin, R. *Acc. Chem. Res.* **2013**, *46*, 1749.
(4) He, L.; Ni, J.; Wang, L.-C.; Yu, F.-J.; Cao, Y.; He, H.-Y.; Fan, K.-N. *Chem. Eur. J.* **2009**, *15*, 11833.
(5) Negishi, Y.; Nobusada, K.; Tsukuda, T. *J. Am. Chem. Soc.* **2005**, *127*, 5261.
(6) Polavarapu, L.; Manna, M.; Xu, Q.-H. *Nanoscale* **2011**, *3*, 429.
(7) Dreaden, E. C.; Alkilany, A. M.; Huang, X.; Murphy, C. J.; El-Sayed, M. A. *Chem. Soc. Rev.* **2012**, *41*, 2740.
(8) Yuan, X.; Setyawati, M.; Leong, D.; Xie, J. *Nano Res.* **2014**, *7*, 301.
(9) Zhu, M.; Aikens, C. M.; Hollander, F. J.; Schatz, G. C.; Jin, R. *J. Am. Chem. Soc.* **2008**, *130*, 5883.
(10) Heaven, M. W.; Dass, A.; White, P. S.; Holt, K. M.; Murray, R. W. *J. Am. Chem. Soc.* **2008**, *130*, 3754.
(11) Desireddy, A.; Conn, B. E.; Guo, J.; Yoon, B.; Barnett, R. N.; Monahan, B. M.; Kirschbaum, K.; Griffith, W. P.; Whetten, R. L.; Landman, U.; Bigioni, T. P. *Nature* **2013**, *501*, 399.
(12) Yang, H.; Wang, Y.; Huang, H.; Gell, L.; Lehtovaara, L.; Malola, S.; Häkkinen, H.; Zheng, N. *Nat. Commun.* **2013**, *4*, 2422.
(13) Kumar, S.; Bolan, M. D.; Bigioni, T. P. *J. Am. Chem. Soc.* **2010**, *132*, 13141.
(14) Dhayal, R. S.; Liao, J.-H.; Liu, Y.-C.; Chiang, M.-H.; Kahlal, S.; Saillard, J.-Y.; Liu, C. W. *Angew. Chem. Int. Ed.* **2015**, *54*, 3702.
(15) AbdulHalim, L. G.; Bootharaju, M. S.; Tang, Q.; del Gobbo, S.; AbdulHalim, R. G.; Eddaoudi, M.; Jiang, D.-e.; Bakr, O. M. *J. Am. Chem. Soc.* **2015**, DOI: 10.1021/jacs.5b04547.
(16) Lopez-Acevedo, O.; Tsunoyama, H.; Tsukuda, T.; Häkkinen, H.; Aikens, C. M. *J. Am. Chem. Soc.* **2010**, *132*, 8210.
(17) Jadzinsky, P. D.; Calero, G.; Ackerson, C. J.; Bushnell, D. A.; Kornberg, R. D. *Science* **2007**, *318*, 430.
(18) Zeng, C.; Chen, Y.; Kirschbaum, K.; Appavoo, K.; Sfeir, M. Y.; Jin, R. *Sci. Adv.* **2015**, *1*, e1500045.
(19) Dass, A.; Theivendran, S.; Nimmala, P. R.; Kumara, C.; Jupally, V. R.; Fortunelli, A.; Sementa, L.; Barcaro, G.; Zuo, X.; Noll, B. C. *J. Am. Chem. Soc.* **2015**, *137*, 4610.
(20) Yang, H.; Wang, Y.; Zheng, N. *Nanoscale* **2013**, *5*, 2674.
(21) Yang, H.; Lei, J.; Wu, B.; Wang, Y.; Zhou, M.; Xia, A.; Zheng, L.; Zheng, N. *Chem. Commun.* **2013**, *49*, 300.
(22) Kumara, C.; Aikens, C. M.; Dass, A. *J. Phys. Chem. Lett.* **2014**, *5*, 461.
(23) Negishi, Y.; Iwai, T.; Ide, M. *Chem. Commun.* **2010**, *46*, 4713.
(24) Teo, B. K.; Keating, K. *J. Am. Chem. Soc.* **1984**, *106*, 2224.
(25) Bakr, O. M.; Amendola, V.; Aikens, C. M.; Wenseleers, W.; Li, R.; Dal Negro, L.; Schatz, G. C.; Stellacci, F. *Angew. Chem. Int. Ed.* **2009**, *121*, 6035.
(26) Bootharaju, M. S.; Burlakov, V. M.; Besong, T. M. D.; Joshi, C. P.; AbdulHalim, L. G.; Black, D.; Whetten, R.; Goriely, A.; Bakr, O. M. *Chem. Mater.* **2015**, *27*, 4289.
(27) Desireddy, A.; Kumar, S.; Guo, J.; Bolan, M. D.; Griffith, W. P.; Bigioni, T. P. *Nanoscale* **2013**, *5*, 2036.
(28) Chakraborty, I.; Govindarajan, A.; Erusappan, J.; Ghosh, A.; Pradeep, T.; Yoon, B.; Whetten, R. L.; Landman, U. *Nano Lett.* **2012**, *12*, 5861.
(29) Aikens, C. M. *J. Phys. Chem. C* **2008**, *112*, 19797.
(30) Dance, I. G.; Fisher, K. J.; Banda, R. M. H.; Scudder, M. L. *Inorg. Chem.* **1991**, *30*, 183.
(31) AbdulHalim, L. G.; Ashraf, S.; Katsiev, K.; Kirmani, A. R.; Kothalawala, N.; Anjum, D. H.; Abbas, S.; Amassian, A.; Stellacci, F.; Dass, A.; Hussain, I.; Bakr, O. M. *J. Mater. Chem. A* **2013**, *1*, 10148.
(32) Conn, B. E.; Desireddy, A.; Atnagulov, A.; Wickramasinghe, S.; Bhattarai, B.; Yoon, B.; Barnett, R. N.; Abdollahian, Y.; Kim, Y. W.; Griffith, W. P.; Oliver, S. R. J.; Landman, U.; Bigioni, T. P. *J. Phys. Chem. C* **2015**, *119*, 11238.
(33) Walter, M.; Akola, J.; Lopez-Acevedo, O.; Jadzinsky, P. D.; Calero, G.; Ackerson, C. J.; Whetten, R. L.; Grönbeck, H.; Häkkinen, H. *Proc. Natl. Acad. Sci.* **2008**, *105*, 9157.
(34) Joshi, C. P.; Bootharaju, M. S.; Bakr, O. M. *J. Phys. Chem. Lett.* **2015**, *6*, 3023.
(35) Tang, Q.; Ouyang, R.; Tian, Z.; Jiang, D.-e. *Nanoscale* **2015**, *7*, 2225.
(36) Tlahuice-Flores, A.; Whetten, R. L.; Jose-Yacaman, M. *J. Phys. Chem. C* **2013**, *117*, 20867.

Table of Contents